Cell

Spatiotemporal Feedback between Actomyosin and Focal-Adhesion Systems Optimizes Rapid Cell Migration

Stephanie L. Gupton[1] and Clare M. Waterman-Storer[1,*]
[1] Department of Cell Biology, The Scripps Research Institute, 10550 North Torrey Pines Road, La Jolla, CA 92037, USA
*Contact: waterman@scripps.edu
DOI 10.1016/j.cell.2006.05.029

SUMMARY

Cells exhibit a biphasic migration-velocity response to increasing adhesion strength, with fast migration occurring at intermediate extracellular matrix (ECM) concentration and slow migration occurring at low and high ECM concentration. A simple mechanical model has been proposed to explain this observation, in which too little adhesion does not provide sufficient traction whereas too much adhesion renders cells immobile. Here we characterize a phenotype for rapid cell migration, which in contrast to the previous model reveals a complex interdependence of subcellular systems that mediates optimal cell migration in response to increasing adhesion strength. The organization and activity of actin, myosin II, and focal adhesions (FAs) are spatially and temporally highly variable and do not exhibit a simple correlation with optimal motility rates. Furthermore, we can recapitulate rapid migration at a nonoptimal ECM concentration by manipulating myosin II activity. Thus, the interplay between actomyosin and FA dynamics results in a specific balance between adhesion and contraction, which induces maximal migration velocity.

INTRODUCTION

Cell migration is described as a four-step cycle that spatially and temporally coordinates forces in the actomyosin cytoskeleton with extracellular adhesion (Lauffenburger and Horwitz, 1996). Actin filaments (F-actin) in migrating epithelial cells are organized into two distinct modules that mediate different steps in the migration cycle (Gupton et al., 2005; Ponti et al., 2004; Salmon et al., 2002). In the first step of migration, a thin lamellipodium protrudes along the leading edge in the direction of migration. The lamellipodium F-actin module is characterized by filament polymerization into a dense network followed by near complete depolymerization at the lamellipodium base (Ponti et al., 2004; Svitkina and Borisy, 1999; Watanabe and Mitchison, 2002). The force produced by polymerization is thought to drive leading-edge protrusion (Pollard and Borisy, 2003) and retrograde flow of F-actin away from the cell edge (Forscher and Smith, 1988; Ponti et al., 2004). In the second step of migration, the protrusion adheres to the extracellular matrix (ECM) by focal adhesions (FAs) that assemble at the lamellipodium base. FAs contain transmembrane integrins that link the ECM to F-actin via structural and signaling proteins (Critchley et al., 1999; Wozniak et al., 2004).

The contractile F-actin module extends from nascent FAs at the lamellipodium base to near the nucleus and is comprised of F-actin-myosin II networks and bundles in the lamella, convergence zone, and central cell area (Salmon et al., 2002). Here, slow myosin II-powered F-actin retrograde flow from the lamella (Gupton et al., 2005; Ponti et al., 2004) and anterograde flow from the central cell region merge in the convergence zone, where F-actin remains stationary and depolymerizes (Vallotton et al., 2004). This myosin II-driven actin convergence is thought to pull on strong FAs at the front to generate traction in the third step of migration and pull on weaker FAs in the rear that detach (Kaverina et al., 2002), moving the cell body forward in the fourth and final step of migration. Importantly, activities of F-actin, myosin II, and FAs within these actin modules must be implemented in a precise place and temporal order to achieve productive, directed cell movement.

Fifteen years ago, a mathematical model predicted that migration speed would exhibit a biphasic response to increasing adhesion strength, with slow migration occurring at low and high strength and fast migration occurring at intermediate strength (DiMilla et al., 1991). The model assumed that migrating cells possess an asymmetry in adhesion strength from front to rear, with front and rear connected by symmetric contractile elements, but did not consider dynamic organizational states of F-actin and FAs. This biphasic dependence of migration velocity on increasing adhesion strength has since been supported experimentally by modulating ECM ligand density,

integrin expression levels, or integrin-ECM binding affinity (DiMilla et al., 1993; Huttenlocher et al., 1996; Palecek et al., 1997), and a front-to-rear gradient in cell adhesion strength has also been demonstrated (Schmidt et al., 1993).

The common explanation for the biphasic migration-velocity response to increased adhesion strength has been simple mechanical effects: At low adhesion, contraction pulls weak FAs at both the cell front and rear from the substrate; at high adhesion, contraction cannot overcome adhesion at the cell front or rear; while at intermediate adhesion, an optimum is reached, with traction generated at the front coupled to adhesion detachment in the rear. However, it is unknown whether adhesion strength spatially or temporally modulates the activities of F-actin, myosin II, or FAs within the lamellipodium or contractile modules to change characteristics of protrusion, adhesion, traction, or deadhesion phases of cell migration. This would be expected since adhesion strength alters signal-transduction pathways that regulate myosin II activity and FA and F-actin assembly/disassembly (Asthagiri et al., 1999; Webb et al., 2004). In addition, spatial and temporal dynamics of F-actin, myosin II, and FAs may be mechanically interdependent (Burridge and Chrzanowska-Wodnicka, 1996). Specifically, myosin II minifilaments are believed to generate tension in F-actin networks (Verkhovsky et al., 1999) to drive the clustering of actin-associated integrins at nascent integrin engagement sites to promote FA formation and maturation (Chrzanowska-Wodnicka and Burridge, 1996; Delanoe-Ayari et al., 2004; Webb et al., 2004). FA formation may immobilize the local actin network via connection to the ECM. Myosin II-dependent tension has been implicated in actomyosin network bundling between these adhesion-immobilized sites to concentrate contractile power into stress fibers (Chrzanowska-Wodnicka and Burridge, 1996). Strongly contractile actomyosin bundles may pull weaker FAs from the ECM (Kaverina et al., 2002; Webb et al., 2004). FA disengagement may then release immobilized F-actin, allowing local debundling and redistribution of myosin II tensile forces in the F-actin network.

Together, these observations suggest that the adhesion-strength dependence of cell migration velocity could arise from spatially and temporally interdependent feedback between F-actin assembly/disassembly and motion, activated myosin II, and FA assembly/disassembly. Furthermore, optimization of cell migration velocity could occur by a specific spatiotemporal state of the actomyosin cytoskeleton and FAs. Here, we used quantitative fluorescent speckle microscopy (qFSM) to test the hypothesis that adhesion strength, modulated by ECM ligand density, affects specific aspects of the organization and dynamics of the lamellipodium and contractile F-actin modules. We used immunofluorescence and live-cell microscopy to determine whether changes in organization and dynamics of myosin II and FA proteins correlate with cell adhesion strength and/or migration velocity. We characterize the unique dynamic organizational state of F-actin, myosin II, and FAs for rapid migration at intermediate adhesion strength and recapitulate fast migration mediated by this specific phenotype at a nonoptimal ECM density by manipulating myosin II activity. Thus, adhesion strength modulates migration speed by spatiotemporal feedback between specific parameters of actomyosin and FA dynamics.

RESULTS

Previous studies have shown that vertebrate cells in culture display maximal migration velocity at intermediate adhesion strength, as modulated by ECM density (DiMilla et al., 1993; Huttenlocher et al., 1996; Palecek et al., 1997). We first established a similar behavior for PtK_1 epithelial cells since we have extensively characterized their F-actin cytoskeleton organization and dynamics (Gupton et al., 2005; Ponti et al., 2004; Wittmann et al., 2003). PtK_1 cells express β_1-integrins (data not shown), which dimerize with α-integrins to form a fibronectin (FN) receptor. PtK_1 cells plated on coverslips coated with increasing FN concentration ([FN]) (0–100 μg/ml) showed increased spreading (Figure 1A), increased cell binding (Figure 1B), and increased adhesion strength (Figure 1C). Migration velocity of cells in small epithelial islands (two to six cells) was measured from time-lapse movies (see Figure 1D and Table S1 in the Supplemental Data available with this article online). Cells plated on coverslips coated with 10 μg/ml FN (0.84 ± 0.02 μm/min) migrated significantly faster than cells plated on higher and lower [FN] (Figure 1D; Table S1; $p < 0.0001$, Tukey's HSD post hoc test [HSD]), recapitulating behavior of other cell types (DiMilla et al., 1993; Palecek et al., 1997).

Leading-Edge Dynamics Do Not Correlate with Biphasic Cell Migration Velocity on Increasing Adhesion Strength

Since protrusion is the first step of migration, we used kymographs of time-lapse movies to analyze leading-edge behavior in cells migrating at various adhesion strengths (Figure 1E; Table S1). Surprisingly, unlike migration velocity, no parameters of protrusion or retraction exhibited a biphasic response to increasing adhesion strength. Specifically, the velocity or persistence of protrusion phases was not significantly altered ($p = 0.7$ and 0.5, respectively, HSD), while the distance of protrusion phases increased with increasing adhesion strength, with significance between some conditions (Table S1; $p < 0.05$ HSD). The duration and distance of retraction phases directly correlated with adhesion strength, while the velocity of retraction phases decreased with higher adhesion (Figure 1F; $p < 0.0001$ HSD). The increase in retraction duration caused a decrease in the frequency of switching from retraction to protrusion at high adhesion strength (Figure 1G). Since retraction parameters were affected by adhesion strength, this suggested that the lamellipodium interacts with the substrate during retraction (Bailly et al., 1998). This was confirmed by comparing edge

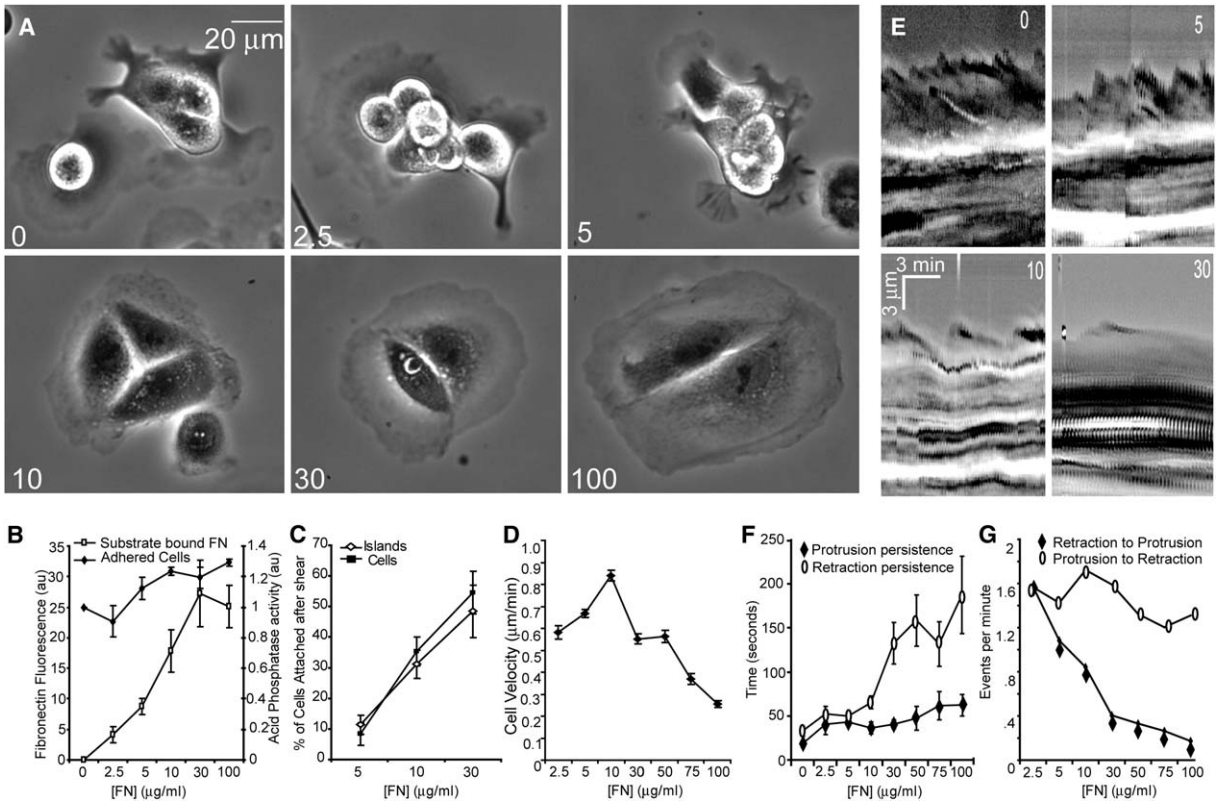

Figure 1. Migration Rate and Leading-Edge Dynamics in Response to Increasing Adhesion to FN

(A) PtK_1 cells 4 hr after plating on coverslips coated with the indicated FN concentration ([FN]) (μg/ml).

(B) FN adhesion to coverslips determined from fluorescent FN (open squares) and number of cells bound 2 hr after plating (black diamonds) with the indicated [FN] (±SD, indicated by acid phosphatase activity to quantify total protein).

(C) Percentage of cells and cell islands remaining attached at different [FN] after 250 dyn/cm^2 fluid shear stress for 10 min (±SEM).

(D) Velocity of cells in small islands migrating on the indicated [FN] (±SEM).

(E) Kymographs from time-lapse phase-contrast images of PtK_1 cells ([FN] for coating in μg/ml in upper right).

(F) Time spent in protrusion and retraction phases versus [FN] (±SEM, n = 20–50 measurements/condition).

(G) Frequency of switching between protrusion and retraction phases versus [FN].

dynamics with total internal reflection fluorescence and wide-field epifluorescence microscopy to determine when the cell edge was close to the substrate (Figure S1). Although no parameters of protrusion correlated with migration velocity, cell migration clearly requires leading-edge advance. Thus, transient edge fluctuations are decoupled from net edge advance.

Adhesion-Strength-Dependent Changes in Migration Velocity Correlate with Changes in the Organization, Kinetics, and Kinematics of the F-Actin Cytoskeleton

To determine whether adhesion-strength-dependent changes in migration rate affected the organization of F-actin dynamics within the lamellipodium and contractile F-actin modules, we performed fluorescent speckle microscopy (FSM) (Danuser and Waterman-Storer, 2003) of cells microinjected with X-rhodamine actin as they migrated at low, intermediate, or high adhesion strength (Figure 1C; 5, 10, and 30 μg/ml FN coating concentrations will be used throughout the study to correspond to low, intermediate, and high [FN], respectively). The lamellipodium is the region of fast retrograde F-actin flow organized in a treadmilling array that resides between the leading edge and the lamella (Ponti et al., 2004; Salmon et al., 2002). FAs initiate at the junction between the lamellipodium and lamella, where F-actin flow velocity slows sharply (Ponti et al., 2004). The contractile module is located between the lamellipodium base and near the nucleus and is composed of the lamella, marked by slow retrograde flow; the central cell area, marked by slow anterograde flow; and the convergence zone at the junction of the lamella and the cell central region, with zero net actin flow (Salmon et al., 2002).

We examined FSM movies to qualitatively evaluate the effects of adhesion strength on these modules (Movie S1). In cells at intermediate and high adhesion strength, the lamellipodium-lamella junction possessed a positionally stable, sharply defined F-actin flow-speed gradient. In contrast, at low adhesion strength, this border was

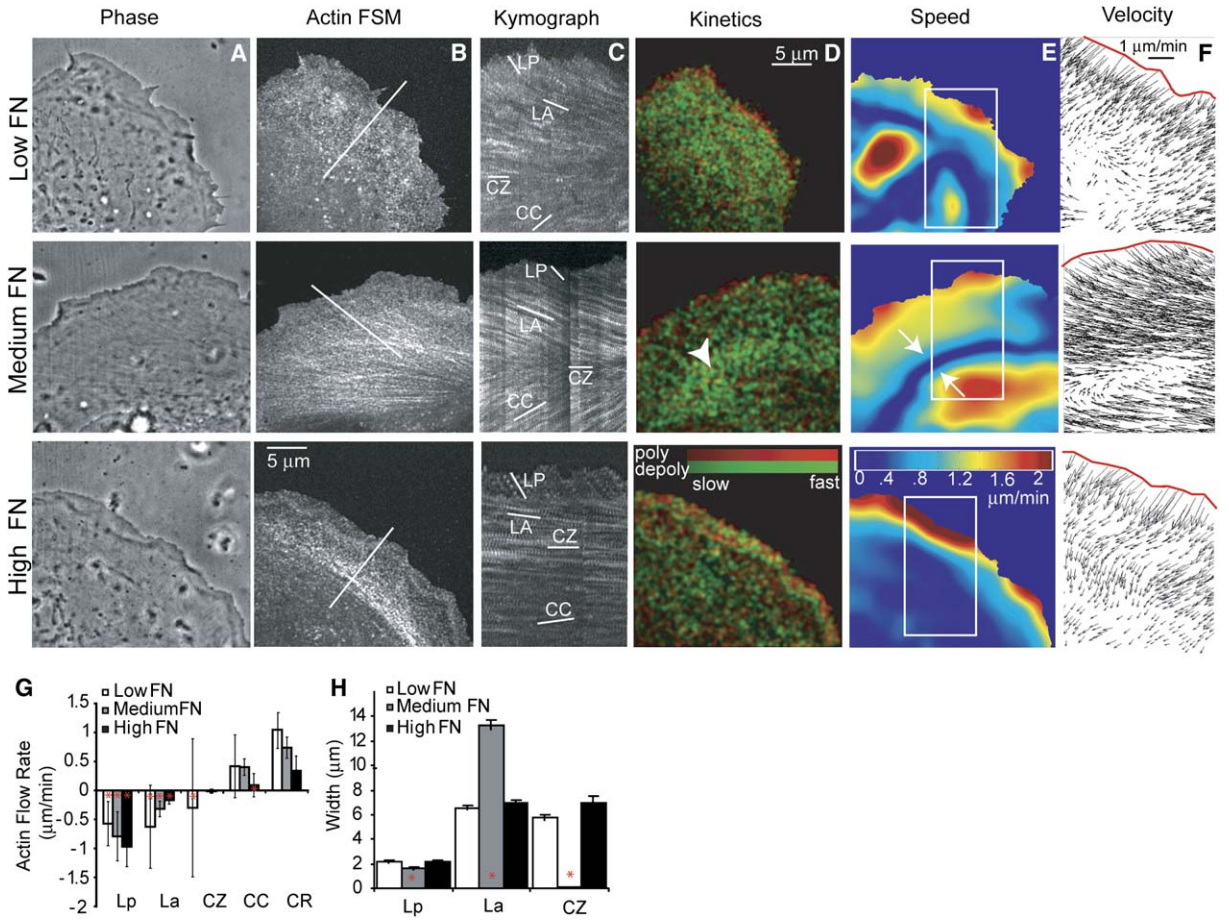

Figure 2. Fast F-Actin Flow Convergence and Depolymerization in the Convergence Zone Correlate with Intermediate Adhesion Strength

(A and B) Phase-contrast (A) and FSM image of X-rhodamine actin (B) in PtK_1 cells migrating on low (5 μg/ml), medium (10 μg/ml), and high (30 μg/ml) [FN].

(C) Kymographs taken from lines oriented along the axis of F-actin flow (highlighted in [B]). Lines in (C) highlight the F-actin speckle flow rate in the lamellipodium (LP), lamella (LA), convergence zone (CZ), and central cell region (CC).

(D) qFSM kinetic maps of F-actin polymerization (red) and depolymerization (green) rates. Brightness indicates relative rate magnitude. Rapid depolymerization occurs in the CZ of the cell on medium [FN] (arrowhead).

(E) qFSM kinematic maps of the speed of F-actin flow. A very thin convergence zone of near zero F-actin flow occurs at medium [FN] (between arrows).

(F) qFSM speckle trajectories from regions indicated by boxes in (E) indicate velocity of F-actin flow.

(G) Average rates of F-actin retrograde (−) or anterograde (+) flow in the lamellipodium (Lp), lamella (La), CZ, CC, and convergence rate (CR) determined from kymographs of FSM movies (±SD).

(H) Average width of cellular regions measured from kymographs (±SEM). Red asterisks in (G) and (H) denote significant differences ($p < 0.05$) between other conditions in the same cellular region (Tukey's HSD post hoc test [HSD]).

variable in position and had a shallower speed gradient. Similarly, in cells at low adhesion strength, F-actin flow in the lamella and cell central region did not meet in a well-defined convergence zone of near zero F-actin flow as at medium and high adhesion strength. Thus, stronger adhesion is required to create or maintain F-actin flow-velocity gradients that define delineation between actin modules in migrating cells.

F-Actin Dynamics in the Lamellipodium

We next used qFSM analysis software to produce spatiotemporal maps of the velocity of F-actin flow (kinematics) and the organization of F-actin assembly/disassembly rates (kinetics) (Ponti et al., 2004). We first examined F-actin kinematics and kinetics in the lamellipodium to determine whether they were modulated by adhesion strength. qFSM and kymograph analysis of kinematics (Figures 2C and 2E; Movie S2) revealed that F-actin retrograde flow velocity in the lamellipodium increased with adhesion strength ($p < 0.0005$ HSD; Figure 2G; Table S2). Lamellipodium width correlated inversely with migration velocity, being narrowest at intermediate adhesion strength ($p < 0.005$ HSD; Figure 2H; Table S2). qFSM

mapping of F-actin assembly/disassembly rates (Figure 2D; Movie S3) revealed that cells at intermediate and high adhesion strength displayed high F-actin polymerization rates (bright red) along the cell edge juxtaposed to rapid depolymerization (bright green). This is indicative of a treadmilling lamellipodium array (Ponti et al., 2004). In contrast, at low adhesion strength, depolymerization spread throughout the cell front, in agreement with our qualitative notion of a poorly defined lamellipodium/lamella junction. Our image-analysis algorithms preclude the ability to compare absolute rates of F-actin kinetics between cells.

F-Actin Dynamics in the Contractile Module

We next analyzed F-actin dynamics in the contractile module in cells at different adhesion strengths. qFSM and kymograph analysis showed that F-actin flow velocity in both the lamella and cell central region decreased significantly with increasing adhesion strength ($p < 0.0005$ HSD; Figures 2C and 2G). At low adhesion, F-actin kinematics in the contractile module were fast and variable (indicated by large standard deviations in flow rates; Figure 2G). At high adhesion strength, F-actin flow in the lamella and central cell region was nearly fully inhibited, with a wide convergence zone of near zero flow rate (Figures 2G and 2H). In contrast, at intermediate adhesion strength, cells displayed well-organized, intermediate-speed retrograde and anterograde flows that met in a narrow zone of zero F-actin flow velocity (Figures 2C and 2E, white arrows; Figure 2F; Movies S1 and S2). In these cells, central anterograde flow was significantly greater than lamella retrograde flow ($p < 0.001$ t test), a front-to-back asymmetry in kinematics not observed at either low or high adhesion strength. Lamella width was significantly larger in cells at intermediate adhesion strength than at low or high strength, while the convergence zone was most narrow at intermediate adhesion strength ($p < 0.0001$ HSD). This indicates that fast cell migration at intermediate adhesion strength correlates with fast F-actin convergence over a small area.

The spatial organization of F-actin assembly/disassembly kinetics was then compared in the contractile module. At all adhesion strengths, there were interspersed punctae of polymerization and depolymerization (Figure 2D; Movie S3), as described (Ponti et al., 2004). Comparison of F-actin kinetic and kinematic maps showed that for cells migrating at intermediate adhesion strength, rapid F-actin depolymerization (bright green) was concentrated in the convergence zone (white arrowhead, Figure 2D). Thus, fast flow convergence is coupled to rapid F-actin depolymerization.

Together, analysis of FSM data shows that a narrow lamellipodium with an intermediate F-actin flow rate and a contractile module consisting of a wide lamella, well-organized, fast, asymmetric F-actin flow convergence, and a narrow zone of zero F-actin flow with rapid filament depolymerization correlate with fast migration at intermediate adhesion strength.

Adhesion Strength Affects Myosin II Distribution and Activity in the Contractile Module

Since F-actin kinematics in the contractile module of migrating epithelial cells are myosin II dependent (Gupton et al., 2002, 2005; Ponti et al., 2004) the adhesion-dependent changes in the contractile module that we observed could be due to changes in myosin II distribution and/or activity. To test this, cytoskeletal bound myosin IIA heavy chain (MHC) and F-actin were localized in prepermeabilized cells at different adhesion strengths (Figures 3A–3C). All cells displayed a gradient of MHC punctae across the contractile module, from very sparse beginning at ~2–4 μm from the leading cell edge (Figure 3A, arrowhead) to extremely dense at ~10–15 μm from the edge and then tapering to near the nucleus (Verkhovsky et al., 1999). The MHC-depleted zone near the cell edge corresponds to the lamellipodium (Gupton et al., 2005; Ponti et al., 2004), while the MHC concentration peak likely corresponds to the convergence zone. To quantitatively compare MHC distribution, fluorescence intensity line scans of MHC immunofluorescence and phalloidin staining were taken normal to the cell edge to the convergence zone. Plots of average intensity versus distance from the edge showed that MHC levels relative to F-actin correlated with migration velocity, with highest levels at intermediate adhesion strength (Figures 3B and 3C; $p < 0.0001$ HSD). In contrast, immunoblotting of cell lysates showed that total MHC was independent of adhesion strength (Figure 3G).

To determine whether myosin II activation correlated with migration velocity, serine 19-phosphorylated myosin II regulatory light chain (pMLC), an indicator of activated myosin II (Adelstein and Conti, 1975), was localized (Figure 3D). Like MHC, pMLC levels relative to F-actin levels were higher across the contractile module at intermediate adhesion strength than at both low and high adhesion (Figures 3E and 3F; $p < 0.0001$ HSD). Immunoblotting of cell lysates showed that total pMLC increased directly with adhesion strength (Figure 3G), in contrast to MHC. pMLC increases mirrored increases in phosphotyrosine levels (Figure S2), suggesting that myosin II activity and signaling from FAs may be coordinated. In summary, increased local myosin II activation in the contractile module correlates with fast migration.

Adhesion Strength Directs the Organization of Focal Adhesions

Presumably, ECM-dependent effects on migration velocity and actomyosin behavior are transmitted mechanically and/or biochemically by FAs. To determine how adhesion strength affects FA morphometry, F-actin and either β_1-integrin, paxillin (a structural and signaling scaffold molecule in FAs), or vinculin (an F-actin binding protein in FAs) were localized in cells at increasing adhesion strength. Similar results were obtained for all three proteins (Figure 4 and data not shown). Cells at low adhesion strength had only peripheral FAs that were often associated with thick peripheral F-actin bundles (Figures 4A and 4B) (Cox et al.,

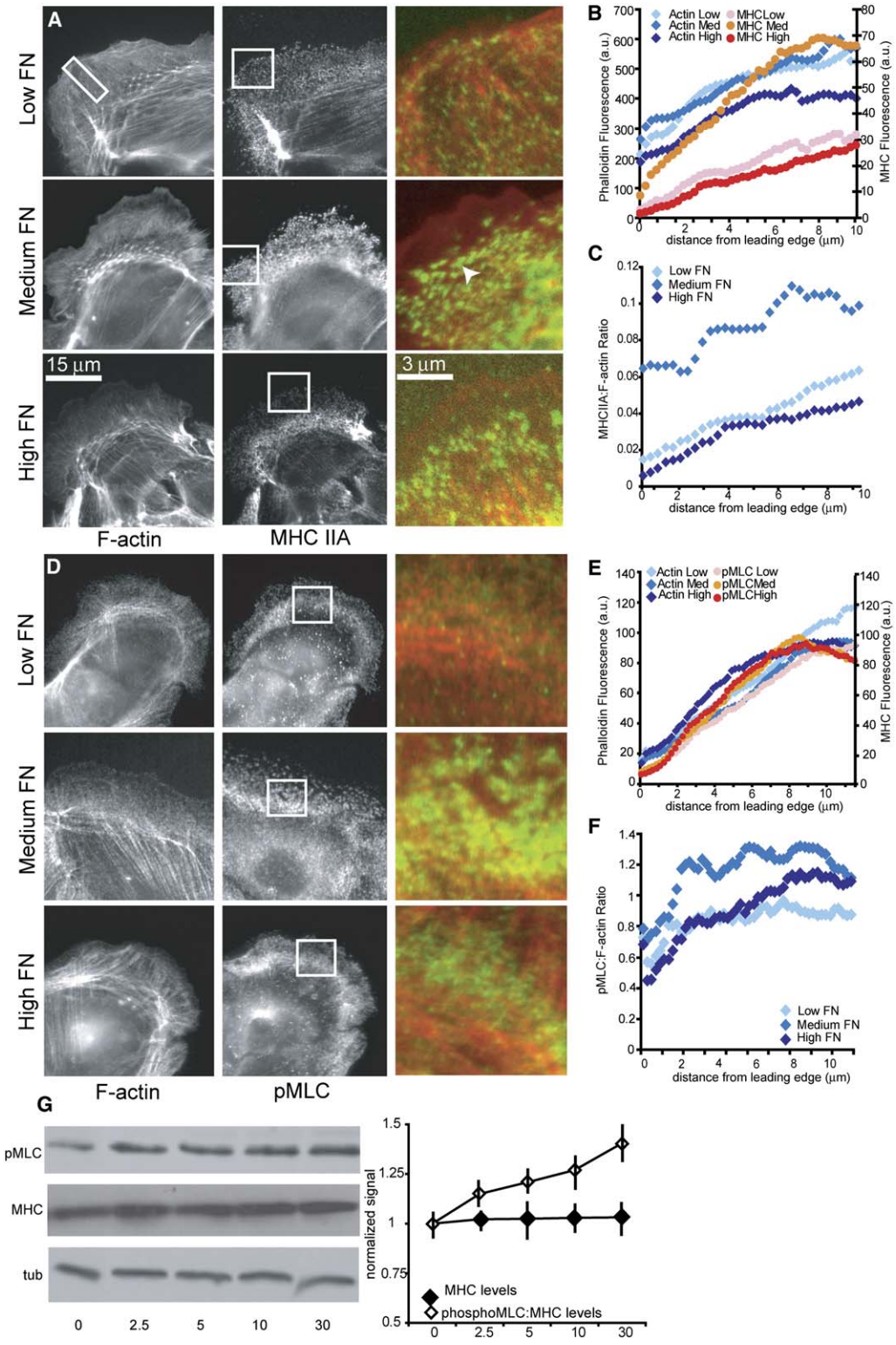

Figure 3. Increased Myosin II Activity across the Lamella Correlates with Intermediate Adhesion Strength

(A) F-actin phalloidin staining and myosin IIA heavy chain (MHC) immunofluorescence in PtK_1 cells migrating on low (5 μg/ml), medium (10 μg/ml), and high (30 μg/ml) [FN]. Merge: F-actin = red, MHC = green. In (A) and (D), boxes in center column indicate position of insets in right column.

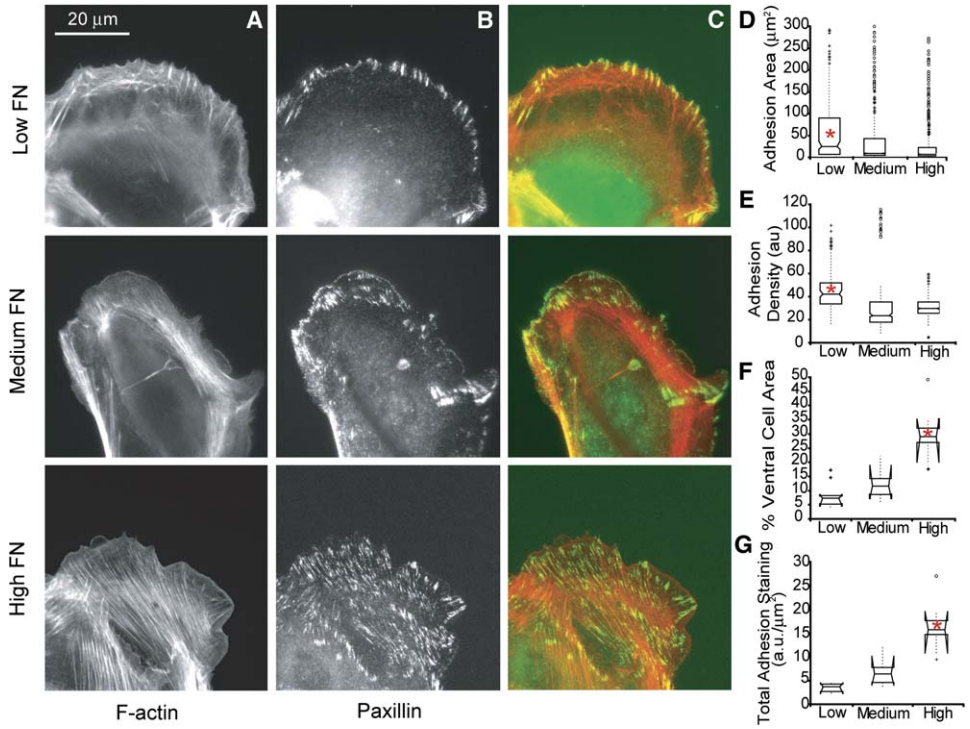

Figure 4. Adhesion Strength Affects the Organization and Density of Paxillin in Focal Adhesions

(A–C) F-actin phalloidin staining (A) and paxillin immunofluorescence (B) in PtK_1 cells on low (5 μg/ml), medium (10 μg/ml), and high (30 μg/ml) [FN]. Merge (C): paxillin = green, phalloidin = red.

(D and E) Plots show the size (D) and density (E) of paxillin staining of individual FAs versus [FN].

(F and G) The percentage of the ventral cell area containing paxillin (F) and the total amount of paxillin in FAs on the ventral cell area (G) versus [FN]. Box and whisker plots in this and subsequent figures indicate the 25th percentile (lower bound), median (middle line), 75th percentile (upper bound), nearest observations within 1.5 times the interquartile range (whiskers), 95% confidence interval of the median (notches), and near (+) and far (0) outliers. Asterisks indicate significant differences from all other [FN] ($p < 0.0001$ HSD).

2001; Huttenlocher et al., 1996). These FAs had significantly greater area and were more densely stained (fluorescence intensity/area, $p < 0.0001$ HSD; Figures 4D and 4E) than in cells at either intermediate or high adhesion. In cells at intermediate adhesion strength, small FAs localized across the lamella and increased in size toward the convergence zone, where F-actin bundles collected in a transverse band (Figures 4A–4C). These FAs were intermediate in size and molecular density. At high adhesion strength, FAs were small, sparsely stained, distributed throughout the ventral cell surface, and connected to many small F-actin bundles spanning the cell (Figure 4). High adhesion strength significantly increased the percentage of the ventral surface area containing FAs ($p < 0.0001$ HSD; Figure 4F), which, when multiplied by the average FA density, revealed a direct relationship between adhesion strength and the total amount of FA molecules at the ventral cell surface ($p < 0.0001$ HSD; Figure 4G). Thus, increased adhesion strength is mediated by increased integrin engagement to the ECM (DiMilla et al., 1991; Palecek et al., 1997) in a spatially specific manner (Cox et al., 2001; Huttenlocher et al., 1996), with

(B) Average relative intensity of F-actin (diamonds; light, medium, and dark blue indicate low, medium, and high [FN], respectively) and MHC staining (circles; pink, orange, and red indicate low, medium, and high [FN], respectively) measured from regions like that boxed in upper left of (A); n = 30 measurements in 10 cells/treatment).

(C) MHC:F-actin fluorescence intensity ratio from the cell edge toward the cell center (light, medium, and dark blue indicate low, medium, and high [FN], respectively).

(D) F-actin phalloidin staining and serine 19-phosphorylated myosin regulatory light chain (pMLC) immunofluorescence in cells on low, medium, and high [FN]. Merge: F-actin = red, pMLC = green.

(E) Average levels of pMLC and F-actin staining. In (E) and (F), the measurement method, analysis, and color scheme of data presentation are the same as in (B) and (C).

(F) pMLC:F-actin fluorescence intensity ratio.

(G) Immunoblot and quantification of MHC and pMLC levels normalized to tubulin (tub) levels from PtK_1 cells on the indicated [FN]. Graph shows averages ± SD from three experiments.

the adhesion strength promoting fastest migration corresponding to FAs of an intermediate size and density distributed across the lamella.

Fast Migration Correlates with Intermediate Focal-Adhesion Lifetime and Rapid Renewal of Focal-Adhesion Components

Two key steps in migration are FA formation and disassembly (Webb et al., 2002). To test whether adhesion strength affected FA kinetics, we imaged migrating cells expressing GFP-paxillin by time-lapse spinning-disk confocal microscopy (Figure 5A; Movie S4) and measured the rate of GFP intensity change in forming or disassembling FAs in the lamella (Webb et al., 2004) (Figures 5B and 5C; Table S2). This revealed that both FA assembly and disassembly rates were inversely correlated with adhesion strength. Specifically, GFP-paxillin intensity increased significantly faster in FAs at low adhesion strength compared to at high adhesion ($p = 0.0065$ HSD) and decreased significantly faster at low adhesion strength than at intermediate and high adhesion ($p < 0.0001$ HSD; Table S1). FA lifetime was measured from the first appearance of a resolvable GFP-paxillin cluster until complete disassembly. FA lifetime increased significantly with adhesion strength ($p < 0.001$, t test low versus medium strength). Indeed, most FAs at high adhesion strength never disassembled in 45 min of imaging (Movie S4), while FAs at low and intermediate strength had an average lifetime of 9.12 ± 1.11 min and 16.98 ± 1.81 min, respectively (Figure 5D). Time-lapse imaging revealed that cells at low adhesion strength often had very small peripheral FAs that were very short lived or rapidly slid and merged with other FAs to make large FAs. These short-lived, small adhesions may not have been apparent in fixed cells where peripheral FAs were large and dense (Figure 4).

FA proteins constantly exchange with the cytoplasmic or membrane-associated pool (Zaidel-Bar et al., 2003; Zimerman et al., 2004). To determine whether this cycling is affected by adhesion strength, we performed fluorescence recovery after photobleaching (FRAP; Figure 6; Movie S5). GFP-α_v-integrin, GFP-vinculin, or GFP-talin (a FA protein that binds β-integrins and F-actin) was expressed in cells with increasing adhesion strength. Single FAs in the lamella were bleached with a 488 nm laser, and fluorescence recovery was recorded. GFP-vinculin and -talin showed complete fluorescence recovery, while GFP-α_v-integrin recovery was incomplete (65%), indicating a nonexchangeable pool within FAs (Table S2). None of these molecules exhibited adhesion-strength-dependent changes in recovery completion (Table S2). To compare molecular dissociation rates, we calculated recovery half-times ($t_{1/2}$). This revealed that GFP-α_v-integrin and GFP-vinculin dissociation correlated with cell migration, as their recovery was significantly faster (lower $t_{1/2}$) at intermediate adhesion strength compared to low or high strength ($p < 0.05$, Fisher's LSD post hoc test for integrin on intermediate versus low and high adhesion strength; $p < 0.05$ and $p < 0.01$, t test for vinculin on intermediate

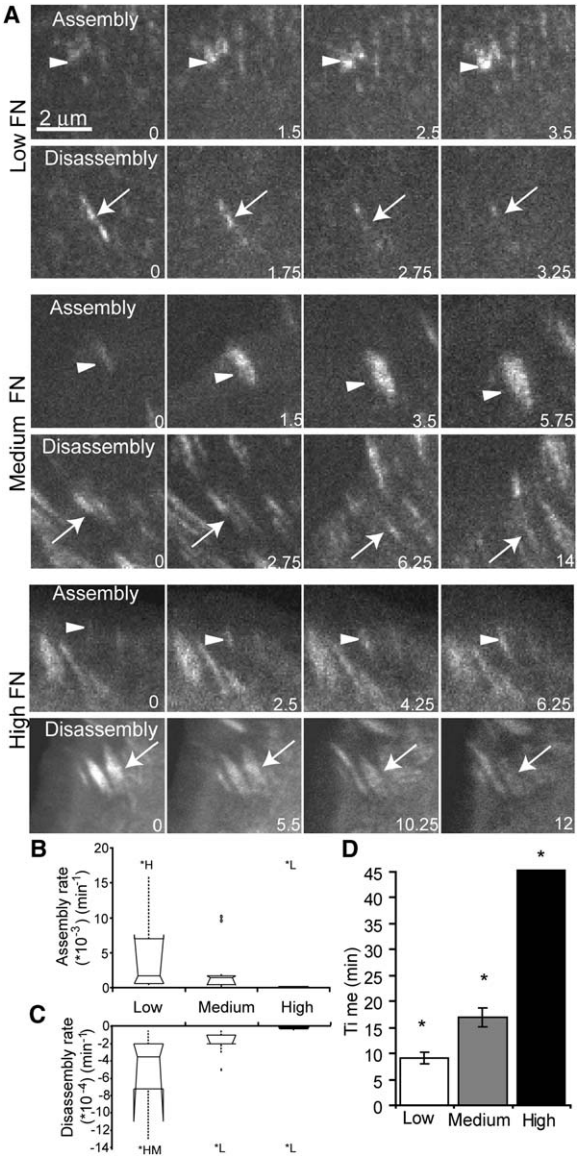

Figure 5. Intermediate Focal-Adhesion Assembly, Disassembly, and Lifetime Correlate with Intermediate Adhesion Strength

(A) Examples of GFP-paxillin fluorescence time-lapse images taken in PtK_1 cells migrating on low (5 μg/ml), medium (10 μg/ml), and high (30 μg/ml) [FN] that were analyzed to determine FA assembly/disassembly rate constants and lifetimes. Arrowheads and arrows indicate assembling and disassembling FAs, respectively. Elapsed time in min is shown.

(B and C) Box and whisker plots (explained in Figure 4) of average rate constants of FA assembly (B) and disassembly (C) measured from 5–20 FAs per cell in 2–3 cells per condition. Asterisks indicate significant differences ($p < 0.01$ HSD) between specified conditions (L, M, and H indicate low, medium, and high [FN], respectively).

(D) Average FA lifetime measured from the initiation of a new GFP-paxillin cluster to complete disappearance. FAs in cells on high [FN] never disassembled within the 45 min of imaging. Asterisks indicate significant differences from all other conditions. Error bars indicate ±SEM.

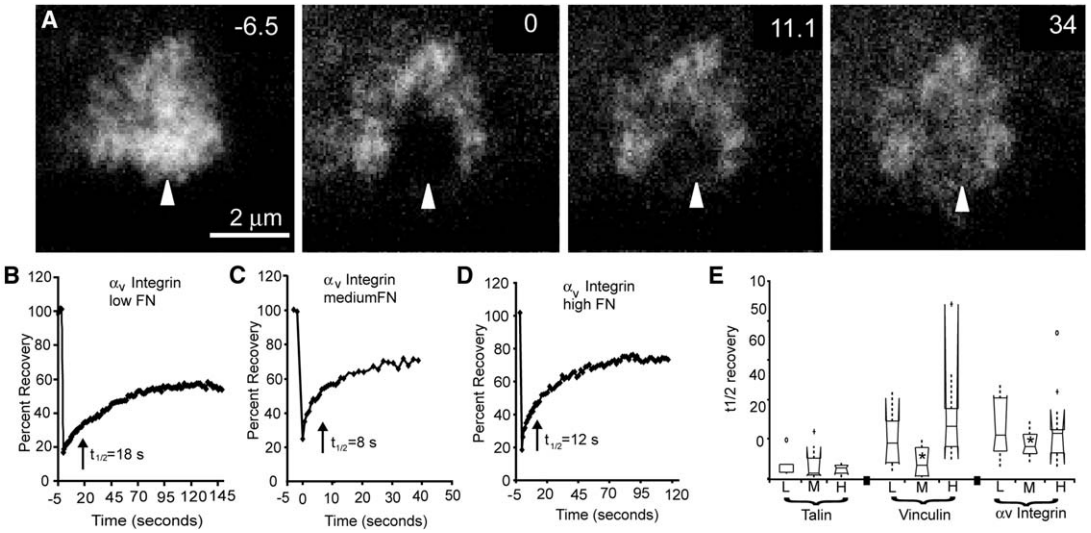

Figure 6. Rapid α_v-Integrin and Vinculin Dissociation from Focal Adhesions Correlates with Intermediate Adhesion Strength

(A) Example of GFP-α_v-integrin FRAP experiment in a PtK_1 cell on low (5 μg/ml) [FN]. Time (in s) relative to laser bleaching (arrowhead) is shown. (B–D) Examples of bleach and recovery curve for α_v-integrin fluorescence in cells migrating on low, medium (10 μg/ml), and high (30 μg/ml) [FN]. (E) Average half-time for fluorescence recovery after bleaching ($t_{1/2}$, s) for GFP-talin, GFP-vinculin, and GFP-α_v-integrin in FAs (n = 1–3 FAs in 4–10 cells per treatment; L, M, and H indicate low, medium, and high [FN] respectively). Asterisks indicate significant differences ($p < 0.05$ HSD) between the same FA component on different [FN].

versus low and high respectively; Figure 6E). GFP-talin fluorescence showed similar recovery times at all adhesion strengths, which were significantly faster than the recovery of GFP-α_v-integrin ($p < 0.0001$ HSD).

Together, these data show that rapid cell migration at intermediate adhesion correlates with intermediate rates of FA assembly, disassembly, and lifetime and with the rapid turnover of the structural components integrin and vinculin within FAs.

Enhancing Myosin II Activity in Cells Migrating at High Adhesion Strength Phenocopies Cells Migrating at Intermediate Adhesion Strength

The above results indicate that fast migration at intermediate adhesion is mediated by a specific dynamic organizational state of F-actin, myosin II, and FAs. Myosin II-mediated contractility is thought to play a pivotal role in actin dynamics and organization and FA formation and turnover. We therefore sought to determine how manipulating myosin II activity affects the relationship between F-actin dynamics, FA morphometry, and cell migration. To decrease myosin II activity, cells were treated with low levels of the myosin II ATPase inhibitor blebbistatin (1 or 5 μM) (Straight et al., 2003). Myosin II activity was enhanced with low levels of calyculin A (CA, 0.5 or 1 nM), a type II phosphatase inhibitor that at low concentrations is relatively specific to myosin light-chain phosphatase (Ishihara et al., 1989), which thus promotes activation of myosin II. These treatments did not alter myosin II distribution, yet they affected its activity (Figure S3).

Analysis of paxillin immunofluorescence revealed that decreasing myosin II activity with blebbistatin at high adhesion strength generated smaller, less dense FAs than in untreated cells at high adhesion ($p < 0.0001$ HSD), although FAs were distributed similarly (Figure 7A). Enhancing myosin II activity with CA at high adhesion strength significantly increased FA size and density and promoted a more peripheral localization compared to untreated cells at high adhesion ($p < 0.0001$ HSD). Treatment with cells on low and medium [FN] induced trends similar to those that we found at high [FN]. These data suggest that increasing myosin contractility promotes FA growth and peripheral distribution.

Since a specific FA size and distribution was associated with rapid migration at intermediate adhesion strength, we wanted to determine whether the myosin II activity level that promoted this FA morphometry at high adhesion also promoted rapid migration (Figure 7D). Indeed, enhanced myosin II activity (0.5 nM CA) at high adhesion increased the migration velocity ($p < 0.0001$ HSD). Either decreasing or enhancing myosin II activity at intermediate adhesion caused significant decreases in velocity ($p < 0.0001$ HSD), suggesting that cells at intermediate adhesion already have optimal contractility for migration (Palecek et al., 1997). Decreasing myosin II activity slightly increased migration velocity at low adhesion ($p = 0.08$, t test). Thus, optimizing myosin II activity overcomes the inhibitory effects of excess or insufficient adhesion strength on cell migration velocity, as was predicted (DiMilla et al., 1991).

To determine whether increased migration speed promoted by enhanced myosin II activity in cells at high adhesion strength correlated with a specific F-actin dynamic organization, qFSM analysis of F-actin was

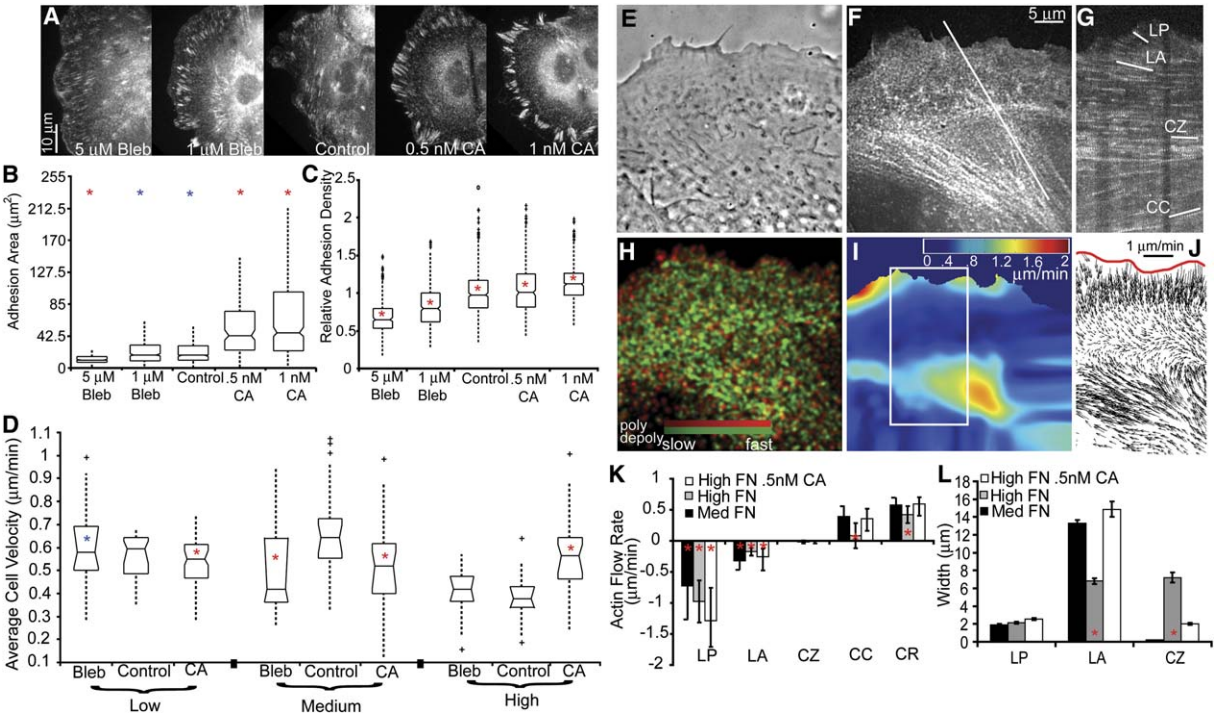

Figure 7. Modulation of Myosin II Activity Alters Focal-Adhesion Organization, Cell Migration Velocity, and F-Actin Behavior

(A) Paxillin immunofluorescence of PtK_1 cells on high (30 µg/ml) [FN] (Control) treated with indicated concentrations of blebbistatin (Bleb) or calyculin A (CA).

(B and C) Quantification of FA size (B) and density (C) in cells on high [FN] treated with Bleb or CA. Red asterisks indicate significant differences between all conditions ($p < 0.0001$ HSD); blue asterisks indicate pairs that are not significantly different from each other.

(D) Migration velocity of cells plated on indicated [FN], treated with 1 µM Bleb, 0.5 nM CA, or left untreated. Red asterisks indicate significant differences between treated and untreated cells ($p < 0.0001$ HSD); blue asterisks indicate statistical significance from untreated cells at 92% confidence (t test).

(E–G) Phase contrast (E), actin FSM (F), and kymograph (G) of a cell on high [FN] treated with 0.5 nM calyculin A.

(H–J) Kinetic (H) and kinematic (I and J) qFSM maps of the rates of F-actin assembly/disassembly (H) (poly = red, depoly = green), speed (I), and velocity (J) of the cell in (E) and (F).

(K and L) Rates of actin flow (K) and region widths (L) in cells on medium and high [FN] and in CA-treated cells on high [FN]. See Figures 2C and 2G for explanation of abbreviations in (K) and (L). Asterisks indicate significant differences between all other treatments ($p < 0.0001$ HSD). Error bars indicate ±SEM.

carried out on cells at high adhesion strength in the presence of 0.5 nM CA (Figures 7E–7L; Movie S6). Remarkably, these cells displayed an actin dynamics phenotype in the contractile module that was indistinguishable from untreated cells at intermediate adhesion. Specifically, compared to untreated cells at high adhesion strength, the contractile module of CA-treated cells had increased rates of F-actin flow in the lamella and cell center, causing increased convergence (Figure 7K; $p < 0.0001$ HSD). They possessed a front-to-back asymmetry in flow rate and a wider lamella and narrower convergence zone where F-actin depolymerization was concentrated (Figures 2K and 2L). CA treatment promoted faster retrograde F-actin flow in the lamellipodium compared to untreated cells at either intermediate or high adhesion strength ($p < 0.0001$ HSD), although lamellipodium width and the treadmilling array were indistinguishable under the three conditions.

Together, these data indicate that F-actin, FAs, and myosin II are interdependent and that a specific balance between myosin II activity and adhesion strength can mediate the generation of a specific FA and F-actin phenotype in the contractile module that correlates with rapid cell migration.

DISCUSSION

The well-established biphasic cell migration-velocity response to increasing adhesion strength was originally predicted by a simple mathematical model in which a positive adhesion gradient from cell front to rear was linked by contractile elements in series. However, unlike assumptions underlying the original model, cell migration is mediated by the interdependent dynamic systems of F-actin, myosin II, and FAs. Here, we dispel the simple model by characterizing dynamic organizational states of each system

at different adhesion strengths and demonstrate the interdependence between organizational states of these systems by establishing how perturbation of one system propagates to changes in the other systems. We show that a specific dynamic organizational state of F-actin, myosin II, and FAs mediates fast epithelial cell migration at intermediate adhesion strength. Manipulating myosin II activity at nonoptimal adhesion recapitulates the specific state, suggesting that a balance between adhesion strength and myosin II activity is required for optimal migration. In the following, we incorporate our findings into a new model. We propose that effects of adhesion strength on FA distribution, combined with local myosin II activity in the contractile module, direct specific spatiotemporal organization states of F-actin. Myosin II contraction then feeds back through a specific F-actin organization to produce a specific pattern of FA turnover, mediating the resulting cell migration velocity.

To promote the general organization of F-actin seen in migrating epithelial cells, we suggest that activated myosin II generates a gradient of convergent tension on F-actin across the contractile module, peaking in the module center. Why and how myosin II is excluded from the lamellipodium and what mediates its spatially specific pattern of assembly are unknown. However, when coupled with filament polymerization at the cell front and center, convergent tension may drive, by a network-contraction mechanism (Verkhovsky et al., 1999), convergent F-actin flows from the lamella and center toward the convergence zone. Concentrated F-actin convergence promotes filament depolymerization, possibly through a mechanical and/or biochemical pathway such as ''solation-contraction coupling'' (Taylor and Fechheimer, 1982). This depolymerization could replenish actin monomers for efficient cytoskeleton remodeling.

The adhesion-dependent variations on this general actomyosin organization that we discovered are likely mediated by FAs. We suggest that FAs nucleate at the base of the lamellipodium by integrin binding to permissive sites on the substrate at a frequency proportional to ECM density. Thus, the total number of FAs is related to ECM density and FA lifetime, as our results suggest. Why FAs form at this location is unknown. However, their initiation may induce local ''engagement'' of flowing F-actin, resulting in the partial immobilization of F-actin relative to the ECM. This creates the flow-speed gradient observed at the lamellipodium/lamella junction at intermediate and high adhesion strengths where FAs were frequent. This gradient was lacking at low adhesion where FAs were sparsely distributed. The degree of F-actin engagement may be dictated by the total number of ECM-coupled ''adhesion units,'' resulting in the inverse relationship between actin flow speed in the contractile module and adhesion strength that we observed.

The myosin II-mediated tension on F-actin engaged at FAs may deform the F-actin network into bundles, as seen in the contractile module. F-actin bundle size may be dictated by the number of actin-engaged adhesion units at a FA, while the F-actin bundle/network organization may be dictated by the distribution and size of FAs. As such, when FAs are large, molecularly dense, and sparsely distributed, as at low adhesion strength, F-actin bundles are large, while when FAs are small, molecularly sparse, and distributed throughout the cell, F-actin bundles are small, frequent, and span the cell, as we saw at high adhesion strength. When FAs form a size gradient across the lamella, F-actin progresses from network organization at the base of the lamellipodium to an increasing bundle-like character in the convergence zone, as seen in cells at intermediate adhesion strength.

We further suggest that the amount of myosin II activity per FA affects FA morphometry and turnover, creating a feedback between these cellular systems that results in the adhesion-strength-dependent effects on cell migration. Once initiated, contraction mediates integrin clustering, FA assembly, and growth of associated actomyosin bundles (Chrzanowska-Wodnicka and Burridge, 1996). Further increases in actomyosin contractility may promote FA turnover by producing more contractile power than the FA can resist. This is supported by our data at high adhesion, where low myosin II activity across the lamella on many small F-actin bundles and FAs would produce a low level of actomyosin contraction per FA, and this correlated with slow FA assembly, long lifetime, and slow disassembly. At low adhesion, although myosin II activity in the lamella was low, there were many fewer FAs, suggesting a high contraction:FA ratio. Thus, the rare FA would be expected to assemble rapidly, possess a large F-actin bundle, disassemble rapidly, and exhibit a short lifetime, as we observed. These data suggest that the lack of FA turnover may inhibit migration at high adhesion strength, while the lack of temporal stabilization of FAs may inhibit migration at low adhesion. In cells migrating at intermediate adhesion strength, higher myosin II activity distributing contractile forces through an F-actin network to an intermediate number of FAs would induce intermediate FA lifetime and turnover rates. Since FAs preferentially form at the lamella front, an intermediate FA lifetime and assembly rate would result in the specific distribution of FAs in a gradient of size across the lamella as seen in cells at intermediate adhesion strength. This would produce a gradient in the contraction:FA ratio across the contractile module, with small new FAs at the cell front resisting low contraction and older FAs at the rear of the contractile module releasing from the ECM, thus driving rapid, efficient cell migration. The FA size gradient would feed back to maintain F-actin organization of the contractile module.

That a specific contraction:adhesion strength ratio can produce this optimized FA morphometry and F-actin dynamic organization was directly demonstrated by enhancing myosin II activity at high adhesion strength (Figure 7). We would predict that cells migrating under these conditions would also have FAs with intermediate kinetics and lifetimes. It will be interesting to determine whether the phenotype we describe here as associated with rapid epithelial cell migration at intermediate adhesion strength is

general for fast migration promoted by other stimuli or in other cell types.

A specific level of myosin II activation per FA may also promote fast FA component renewal within FAs (Figure 6). Contraction could pull specific components that are structurally linked to F-actin out of FAs, similar to how contraction is thought to drive clustering of integrins to promote FA growth (Brunton et al., 2004). Indeed, we found that α_v-integrin and vinculin rapidly turn over within FAs at intermediate adhesion strength. In surprising contrast, talin, thought to be a load-bearing link between F-actin and β-integrin, did not exhibit adhesion-strength-dependent changes in turnover rates, suggesting that this link may be critical to cell adhesion but not to migration velocity.

This model provides one possible explanation for the adhesion-strength-dependent modulation of cell migration velocity considering only mechanical integration of F-actin, myosin II, and FAs. It is well established that integrin engagement induces activation of signaling pathways affecting these cellular systems. For example, adhesion strength modulates the activity of Rho family GTPases and MAP, ERK2, and FAK kinases (Asthagiri et al., 1999; Cox et al., 2001; Holub et al., 2003; Huttenlocher et al., 1996). Modulation of ERK2 signaling could be responsible for adhesion-strength-dependent modulation of myosin II activation, while FAK and ERK could regulate FA disassembly (Webb et al., 2004). Integrin-mediated activation of Rac1 (del Pozo et al., 2003), a regulator of Arp2/3 and ADF-cofilin in the lamellipodium, could mediate the adhesion-dependent changes in F-actin that we observed. These pathways could also feed back to adhesion strength via inside-out modulation of integrin-ECM affinity (Brunton et al., 2004). Mechanical regulation of signal transduction occurs for Rho family GTPases (Katsumi et al., 2002), induces conformational changes in proteins to regulate ion channels (Hamill and Martinac, 2001), and uncovers binding sites for adaptor and signaling proteins (Tamada et al., 2004). Thus, it is likely that mechanics and signaling are coupled or synergistic in mediating the feedback between adhesion strength and F-actin, myosin II, and FA dynamics to modulate cell migration velocity.

EXPERIMENTAL PROCEDURES

Cell Culture and Microinjection

PtK_1 cells were plated for 12–16 hr before experiments in F-12 media (Sigma) with 1% fetal bovine serum (GIBCO) on FN-coated #1.5 coverslips prepared as described (de Rooij et al., 2005). Cells were microinjected with X-rhodamine-conjugated actin or plasmid DNA as described (Gupton et al., 2005). GFP-α_v-integrin was coexpressed with unlabeled β_3-integrin. Cells were prepared for live-cell microscopy as described (Gupton et al., 2005).

Adhesion Assays

To determine the relative number of adherent cells, experiments were performed in quadruplicate as described (de Rooij et al., 2005). To measure relative adhesion strength of PtK_1 cells, a laminar flow system was used to impose 250 dyn/cm^2 shear stress as described previously (Frangos et al., 1985). Briefly, cells were cultured overnight on 75 × 25 mm glass slides coated with FN. A silicone gasket was sandwiched between the glass slide and an acrylic plate to create a rectangular flow channel (125 μm × 1.0 cm × 5.0 cm). Laminar flow was generated using a fluid reservoir, peristaltic pump, and damper reservoir within a 37°C cabinet. The number of cells and cell islands at each FN concentration were counted before and after subjection to laminar flow.

Immunofluorescence and Immunoblotting

Cells were fixed and processed for immunofluorescence as described (Gupton et al., 2005) using Cy2 secondary antibodies and Alexa 568 phalloidin for staining F-actin. Cells were lysed directly in sample buffer, and immunoblots were developed with ECL (Amersham). Antibodies were obtained from the following sources. pMLC: Dr. Y. Sasaki, Kitasito University, Tokyo, Japan; myosin IIA heavy chain, Biomedical Technologies, Inc.; phosphotyrosine and paxillin, Signal Transduction Laboratories; human vinculin, Sigma; β1-integrin, Endogen.

Microscopy

F-actin FSM and phase-contrast time-lapse image series were acquired at 5–10 s intervals using a 100×/1.4 NA Plan Apo phase objective lens (Nikon) on a spinning-disk confocal microscope (Adams et al., 2003). GFP-paxillin images were acquired at 15 s intervals using the same system. Leading-edge activity and cell migration rates were determined from phase-contrast time series acquired on an inverted microscope system (de Rooij et al., 2005) using a 20×/0.5 NA Plan Apo phase objective lens (Nikon). For cell velocity, images were captured every 2 min for 8 hr; for leading-edge characterization, every 10 s for 10 min. Epifluorescence images of fixed cells were acquired on an inverted microscope system (Wittmann et al., 2003) using a 60×/1.4 NA Plan Apo DIC objective lens (Nikon). FRAP was performed using a DeltaVision RT microscope system equipped with a 50 mW Ar laser, a 100×/1.4 NA Plan Apo phase-contrast objective lens (Olympus), and a Roper Coolsnap camera or an inverted microscope (TE2000E Nikon) in which the 488 nm line of a KrAr laser (2.5 W, Spectraphysics) was introduced fiber-optically into a Nikon FRAP illuminator and images were collected with a 60×/1.4 NA Plan Apo DIC objective lens (Nikon) on a spinning-disk confocal scanner (Yokogawa) using a Hamamatsu Orca ER camera. FAs were bleached by the laser focused to a diffraction-limited spot; fluorescence recovery was imaged at 0.5–2 s intervals for 10 min.

Image Analysis

Leading-edge behavior and cell migration velocity were analyzed as described (Gupton et al., 2005). F-actin flow rates were measured by kymograph analysis (Waterman-Storer, 2002). Flow maps were produced with qFSM software (Ponti et al., 2004). The boundary between zones was defined as sites of flow speed or direction change as seen on kymographs. The lamellipodium/lamella border was delineated by a negative flow-speed gradient, the convergence zone was the region of zero F-actin flow velocity bounded by a negative flow-speed gradient on the cell-edge-facing side and a positive flow-speed gradient on the cell-center-facing side, and the lamella was delineated by boundaries with the lamellipodium and the convergence zone.

F-actin polymerization and depolymerization maps were calculated using qFSM software (Ponti et al., 2003; Vallotton et al., 2003). Fluorescence intensity line-scan measurements of F-actin, myosin IIA, and pMLC were performed as described (Gupton et al., 2005). FA density and area measurements were performed in Metamorph by thresholding paxillin immunofluorescence images to include only FAs. All images were background subtracted prior to intensity measurements. Ventral cell area was measured by tracing the outline of the phalloidin-stained cell. Quantification of FA dynamics was performed for image series of GFP-paxillin as described (Webb et al., 2004). For analysis of photobleaching recovery, the integrated fluorescence intensity inside a region smaller than the original bleach region was recorded in prebleach and recovery image series. Calculations of the percent recovery and $t_{1/2}$ of recovery was performed as described (Bulinski et al., 2001).

Statistical Analysis

For multiple conditions, we compared means by analysis of variance (ANOVA). All data found to be significant by ANOVA were compared with Tukey's HSD or Fisher's LSD (depending on the number of groups) post hoc test to reveal statistically different groups. Statistical differences between two conditions were determined using Student's t test.

Supplemental Data

Supplemental Data include three figures, two tables, and six movies and can be found with this article online at http://www.cell.com/cgi/content/full/125/7/1361/DC1/.

ACKNOWLEDGMENTS

We thank Y. Sasaki for antibodies; D. Webb for GFP-paxillin and GFP-α_v-integrin; A. Huttenlocher for GFP-talin; M. Ginsberg for β_3-integrin; Applied Precision Instruments for use of the DeltaVision RT system; P. Maddox and A. Desai for use of their FRAP microscope; S. Chien and J. Li for use of their shear stress chamber; C. Lanigan for help with statistical analysis; and J. de Rooij, K. Hu, M. Gardel, and members of the Waterman and Danuser labs for technical advice and thoughtful discussion. Supported by NIH grant GM67230 to C.M.W.-S. and a HHMI predoctoral fellowship to S.L.G.

Received: August 26, 2005
Revised: January 11, 2006
Accepted: May 18, 2006
Published: June 29, 2006

REFERENCES

Adams, M.C., Salmon, W.C., Gupton, S.L., Cohan, C.S., Wittmann, T., Prigozhina, N., and Waterman-Storer, C.M. (2003). A high-speed multispectral spinning-disk confocal microscope system for fluorescent speckle microscopy of living cells. Methods *29*, 29–41.

Adelstein, R.S., and Conti, M.A. (1975). Phosphorylation of platelet myosin increases actin-activated myosin ATPase activity. Nature *256*, 597–598.

Asthagiri, A.R., Nelson, C.M., Horwitz, A.F., and Lauffenburger, D.A. (1999). Quantitative relationship among integrin-ligand binding, adhesion, and signaling via focal adhesion kinase and extracellular signal-regulated kinase 2. J. Biol. Chem. *274*, 27119–27127.

Bailly, M., Yan, L., Whitesides, G.M., Condeelis, J.S., and Segall, J.E. (1998). Regulation of protrusion shape and adhesion to the substratum during chemotactic responses of mammalian carcinoma cells. Exp. Cell Res. *241*, 285–299.

Brunton, V.G., MacPherson, I.R., and Frame, M.C. (2004). Cell adhesion receptors, tyrosine kinases and actin modulators: a complex three-way circuitry. Biochim. Biophys. Acta *1692*, 121–144.

Bulinski, J.C., Odde, D.J., Howell, B.J., Salmon, T.D., and Waterman-Storer, C.M. (2001). Rapid dynamics of the microtubule binding of ensconsin in vivo. J. Cell Sci. *114*, 3885–3897.

Burridge, K., and Chrzanowska-Wodnicka, M. (1996). Focal adhesions, contractility, and signaling. Annu. Rev. Cell Dev. Biol. *12*, 463–518.

Chrzanowska-Wodnicka, M., and Burridge, K. (1996). Rho-stimulated contractility drives the formation of stress fibers and focal adhesions. J. Cell Biol. *133*, 1403–1415.

Cox, E.A., Sastry, S.K., and Huttenlocher, A. (2001). Integrin-mediated adhesion regulates cell polarity and membrane protrusion through the Rho family of GTPases. Mol. Biol. Cell *12*, 265–277.

Critchley, D.R., Holt, M.R., Barry, S.T., Priddle, H., Hemmings, L., and Norman, J. (1999). Integrin-mediated cell adhesion: the cytoskeletal connection. Biochem. Soc. Symp. *65*, 79–99.

Danuser, G., and Waterman-Storer, C.M. (2003). Quantitative fluorescent speckle microscopy: where it came from and where it is going. J. Microsc. *211*, 191–207.

Delanoe-Ayari, H., Al Kurdi, R., Vallade, M., Gulino-Debrac, D., and Riveline, D. (2004). Membrane and acto-myosin tension promote clustering of adhesion proteins. Proc. Natl. Acad. Sci. USA *101*, 2229–2234.

del Pozo, M.A., Schwartz, M.A., Hu, J., Kiosses, W.B., Altman, A., and Villalba, M. (2003). Guanine exchange-dependent and -independent effects of Vav1 on integrin-induced T cell spreading. J. Immunol. *170*, 41–47.

de Rooij, J., Kerstens, A., Danuser, G., Schwartz, M.A., and Waterman-Storer, C.M. (2005). Integrin-dependent actomyosin contraction regulates epithelial cell scattering. J. Cell Biol. *171*, 153–164.

DiMilla, P.A., Barbee, K., and Lauffenburger, D.A. (1991). Mathematical model for the effects of adhesion and mechanics on cell migration speed. Biophys. J. *60*, 15–37.

DiMilla, P.A., Stone, J.A., Quinn, J.A., Albelda, S.M., and Lauffenburger, D.A. (1993). Maximal migration of human smooth muscle cells on fibronectin and type IV collagen occurs at an intermediate attachment strength. J. Cell Biol. *122*, 729–737.

Forscher, P., and Smith, S.J. (1988). Actions of cytochalasins on the organization of actin filaments and microtubules in a neuronal growth cone. J. Cell Biol. *107*, 1505–1516.

Frangos, J.A., Eskin, S.G., McIntire, L.V., and Ives, C.L. (1985). Flow effects on prostacyclin production by cultured human endothelial cells. Science *227*, 1477–1479.

Gupton, S.L., Salmon, W.C., and Waterman-Storer, C.M. (2002). Converging populations of f-actin promote breakage of associated microtubules to spatially regulate microtubule turnover in migrating cells. Curr. Biol. *12*, 1891–1899.

Gupton, S.L., Anderson, K.L., Kole, T.P., Fischer, R.S., Ponti, A., Hitchcock-DeGregori, S.E., Danuser, G., Fowler, V.M., Wirtz, D., Hanein, D., and Waterman-Storer, C.M. (2005). Cell migration without a lamellipodium: translation of actin dynamics into cell movement mediated by tropomyosin. J. Cell Biol. *168*, 619–631.

Hamill, O.P., and Martinac, B. (2001). Molecular basis of mechanotransduction in living cells. Physiol. Rev. *81*, 685–740.

Holub, A., Byrnes, J., Anderson, S., Dzaidzio, L., Hogg, N., and Huttenlocher, A. (2003). Ligand density modulates eosinophil signaling and migration. J. Leukoc. Biol. *73*, 657–664.

Huttenlocher, A., Ginsberg, M.H., and Horwitz, A.F. (1996). Modulation of cell migration by integrin-mediated cytoskeletal linkages and ligand-binding affinity. J. Cell Biol. *134*, 1551–1562.

Ishihara, H., Ozaki, H., Sato, K., Hori, M., Karaki, H., Watabe, S., Kato, Y., Fusetani, N., Hashimoto, K., Uemura, D., et al. (1989). Calcium-independent activation of contractile apparatus in smooth muscle by calyculin-A. J. Pharmacol. Exp. Ther. *250*, 388–396.

Katsumi, A., Milanini, J., Kiosses, W.B., del Pozo, M.A., Kaunas, R., Chien, S., Hahn, K.M., and Schwartz, M.A. (2002). Effects of cell tension on the small GTPase Rac. J. Cell Biol. *158*, 153–164.

Kaverina, I., Krylyshkina, O., and Small, J.V. (2002). Regulation of substrate adhesion dynamics during cell motility. Int. J. Biochem. Cell Biol. *34*, 746–761.

Lauffenburger, D.A., and Horwitz, A.F. (1996). Cell migration: a physically integrated molecular process. Cell *84*, 359–369.

Palecek, S.P., Loftus, J.C., Ginsberg, M.H., Lauffenburger, D.A., and Horwitz, A.F. (1997). Integrin-ligand binding properties govern cell migration speed through cell-substratum adhesiveness. Nature *385*, 537–540.

Pollard, T.D., and Borisy, G.G. (2003). Cellular motility driven by assembly and disassembly of actin filaments. Cell *112*, 453–465.

Ponti, A., Vallotton, P., Salmon, W.C., Waterman-Storer, C.M., and Danuser, G. (2003). Computational analysis of F-actin turnover in cortical actin meshworks using fluorescent speckle microscopy. Biophys. J. *84*, 3336–3352.

Ponti, A., Machacek, M., Gupton, S.L., Waterman-Storer, C.M., and Danuser, G. (2004). Two distinct actin networks drive the protrusion of migrating cells. Science *305*, 1782–1786.

Salmon, W.C., Adams, M.C., and Waterman-Storer, C.M. (2002). Dual-wavelength fluorescent speckle microscopy reveals coupling of microtubule and actin movements in migrating cells. J. Cell Biol. *158*, 31–37.

Schmidt, C.E., Horwitz, A.F., Lauffenburger, D.A., and Sheetz, M.P. (1993). Integrin-cytoskeletal interactions in migrating fibroblasts are dynamic, asymmetric, and regulated. J. Cell Biol. *123*, 977–991.

Straight, A.F., Cheung, A., Limouze, J., Chen, I., Westwood, N.J., Sellers, J.R., and Mitchison, T.J. (2003). Dissecting temporal and spatial control of cytokinesis with a myosin II Inhibitor. Science *299*, 1743–1747.

Svitkina, T.M., and Borisy, G.G. (1999). Arp2/3 complex and actin depolymerizing factor/cofilin in dendritic organization and treadmilling of actin filament array in lamellipodia. J. Cell Biol. *145*, 1009–1026.

Tamada, M., Sheetz, M.P., and Sawada, Y. (2004). Activation of a signaling cascade by cytoskeleton stretch. Dev. Cell *7*, 709–718.

Taylor, D.L., and Fechheimer, M. (1982). Cytoplasmic structure and contractility: the solation–contraction coupling hypothesis. Philos. Trans. R. Soc. Lond. B Biol. Sci. *299*, 185–197.

Vallotton, P., Ponti, A., Waterman-Storer, C.M., Salmon, E.D., and Danuser, G. (2003). Recovery, visualization, and analysis of actin and tubulin polymer flow in live cells: a fluorescent speckle microscopy study. Biophys. J. *85*, 1289–1306.

Vallotton, P., Gupton, S.L., Waterman-Storer, C.M., and Danuser, G. (2004). Simultaneous mapping of filamentous actin flow and turnover in migrating cells by quantitative fluorescent speckle microscopy. Proc. Natl. Acad. Sci. USA *101*, 9660–9665.

Verkhovsky, A.B., Svitkina, T.M., and Borisy, G.G. (1999). Network contraction model for cell translocation and retrograde flow. Biochem. Soc. Symp. *65*, 207–222.

Watanabe, N., and Mitchison, T.J. (2002). Single-molecule speckle analysis of actin filament turnover in lamellipodia. Science *295*, 1083–1086.

Waterman-Storer, C. (2002). Fluorescent speckle microscopy (FSM) of microtubules and actin in living cells. In Current Protocols in Cell Biology, J.S. Bonifacino, M. Dasso, J.B. Harford, J.L. Schwartz, and K.M. Yamada, eds. (Hoboken, NJ, USA: John Wiley & Sons), pp. 4.10.1–4.10.26.

Webb, D.J., Parsons, J.T., and Horwitz, A.F. (2002). Adhesion assembly, disassembly and turnover in migrating cells—over and over and over again. Nat. Cell Biol. *4*, E97–E100.

Webb, D.J., Donais, K., Whitmore, L.A., Thomas, S.M., Turner, C.E., Parsons, J.T., and Horwitz, A.F. (2004). FAK-Src signalling through paxillin, ERK and MLCK regulates adhesion disassembly. Nat. Cell Biol. *6*, 154–161.

Wittmann, T., Bokoch, G.M., and Waterman-Storer, C.M. (2003). Regulation of leading edge microtubule and actin dynamics downstream of Rac1. J. Cell Biol. *161*, 845–851.

Wozniak, M.A., Modzelewska, K., Kwong, L., and Keely, P.J. (2004). Focal adhesion regulation of cell behavior. Biochim. Biophys. Acta *1692*, 103–119.

Zaidel-Bar, R., Ballestrem, C., Kam, Z., and Geiger, B. (2003). Early molecular events in the assembly of matrix adhesions at the leading edge of migrating cells. J. Cell Sci. *116*, 4605–4613.

Zimerman, B., Volberg, T., and Geiger, B. (2004). Early molecular events in the assembly of the focal adhesion-stress fiber complex during fibroblast spreading. Cell Motil. Cytoskeleton *58*, 143–159.